Protein Science (1998), 7:1106–1115. Cambridge University Press. Printed in the USA.

Hinge bending within the cytokine receptor superfamily revealed by the 2.4 Å crystal structure of the extracellular domain of rabbit tissue factor

YVES A. MULLER,[1] ROBERT F. KELLEY,[2] AND ABRAHAM M. DE VOS[2]

[1]Forschungsgruppe Kristallographie, Max-Delbrück-Centrum für Molekulare Medizin, Robert-Rössle-Straße 10, D-13122 Berlin-Buch, Germany

[2]Department of Protein Engineering, Genentech, Inc., 460 Point San Bruno Boulevard, South San Francisco, California 94080

(RECEIVED December 3, 1997; ACCEPTED January 22, 1998)

Abstract

Tissue factor (TF), a member of the cytokine receptor superfamily, is the obligate cofactor of coagulation factor VIIa (FVIIa), and has a pivotal role in initiating the extrinsic pathway of blood coagulation through formation of the TF·FVIIa complex. The crystal structure of the extracellular portion of rabbit TF has been solved at 2.35 Å resolution and refined to a crystallographic *R*-value of 19.1% (free *R*-value, 27.7%). Like the human homologue, the extracellular portion consists of two fibronectin type III domains connected by a short α-helical segment. Unexpectedly, the two molecules in the crystallographic asymmetric unit differ in their relative domain–domain orientation, revealing unsuspected hinge motion consisting of a rotation of about 12.7° around an axis intersecting the linker segment at residue 106. Superposition of rabbit tissue factor with free and bound human tissue factor allows for the detection of an identical, albeit smaller, hinge motion in human TF induced upon binding of FVIIa. This raises the possibility that a very similar hinge axis may be present in other members of the cytokine receptor superfamily.

Keywords: blood coagulation; domain–domain flexibility; FVIIa activation; FVIIa specificity; hematopoietic receptor superfamily

Tissue factor (TF), the obligate cofactor of the plasma serine protease factor VIIa (FVIIa), initiates the extrinsic pathway of blood coagulation (Davie et al., 1991). Tissue factor is an integral membrane protein and is normally expressed on cells of the tissue adventitia. Upon vascular damage, FVIIa present in plasma forms a calcium-dependent high-affinity complex with TF. The complex TF·FVIIa then auto-activates factor VII, and activates the serine proteases factors X and IX, ultimately leading to the conversion of fibrinogen to fibrin and the deposition of a clot. TF functions as an essential cofactor, enhancing the proteolytic activity of FVIIa about 10^5-fold (Bom & Bertina, 1990). Testing of anti-TF antibodies in animal models suggests an important role of TF in the pathophysiology of thrombosis (Pawashe et al., 1994) and sepsis (Taylor et al., 1991). Therefore, molecules designed to inhibit the formation or activity of the TF·FVIIa complex might have considerable therapeutic potential.

Tissue factor consists of a 219-residue extracellular portion, a membrane-spanning single α-helix (23 residues), and a short cytoplasmic domain (21 residues) (Morrissey et al., 1987; Scarpati et al., 1987). Considerable insight into how TF activates FVIIa has been gained from the crystal structures of the extracellular portion of human TF (h-TF) alone (Harlos et al., 1994; Muller et al., 1994, 1996) and in complex with FVIIa (Banner et al., 1996), as well as from extensive mutational studies (Kelley et al., 1995; Dickinson et al., 1996). In the present understanding, tissue factor functions as a rigid scaffold, and binding of FVIIa to TF locks FVIIa in an active conformation. This model is corroborated by the observation that the inhibition strength of FVIIa active-site inhibitors correlates with the affinity of inhibited FVIIa for TF (Higashi et al., 1996). Although the observed conformation of FVIIa in the TF·FVIIa complex is similar to the conformation of other active serine proteases, the conformation of unbound FVIIa remains unknown.

Sequence alignments (Bazan, 1990) as well as the crystal structures show that TF is a member of the cytokine receptor family. To date, a number of other cytokine receptors have been extensively studied and their crystal structures elucidated, but only in complex with their respective ligands (Wells & de Vos, 1996). In recent

Reprint requests to: Yves A. Muller, Forschungsgruppe Kristallographie, Max-Delbrück-Centrum für Molekulare Medizin, Robert-Rössle-Straße 10, D-13122 Berlin-Buch, Germany; e-mail: yam@mdc-berlin.de.

Abbreviations: TF, tissue factor; r-TF, rabbit TF; h-TF, human TF; FVIIa, plasma coagulation factor VIIa; r-TF_A and r-TF_B, molecules A and B of r-TF in the crystallographic asymmetric unit; h-TF_{Free} and h-TF_{FVIIa}, h-TF as observed in the crystal structure of h-TF by itself and in complex with FVIIa; FNIII, fibronectin type III.

years evidence has emerged that in addition to its cofactor role for factor FVIIa, TF might be directly involved in cell signaling events (Zioncheck et al., 1992; Rottingen et al., 1995); however, the mechanism remains elusive.

The soluble form of the K165A, K166A double mutant of h-TF, termed "hTFAA," was recently shown to function as a selective antagonist of the extrinsic pathway of blood coagulation (Kelley et al., 1997). The two mutations result in decreased cofactor function in support of factor X activation but have no effect on FVIIa binding. hTFAA produces an antithrombotic effect in a rabbit model of arterial thrombosis; however, high doses are required to produce the effect, in part because hTFAA is a 70-fold less potent anticoagulant with rabbit plasma than with human plasma. The rabbit homologue of hTFAA, "rTFAA," is a more potent inhibitor in rabbit plasma, and lower doses suffice to produce an antithrombotic effect in the rabbit thrombosis model. The present crystallographic investigation was initiated to gain structural insight into the species specificity of this class of coagulation inhibitors.

Results and discussion

Accuracy of the model

The structure of the extracellular portion of rabbit TF (r-TF) was solved at 2.35 Å resolution and refined to a crystallographic *R*-value of 19.1% (and a free *R*-value of 27.7%, Table 1). The mean coordinate error as calculated from Luzzati (Luzzati, 1952) and Sigmaa (Read, 1986) plots is between 0.2 and 0.3 Å. The crystals contain two independent copies of r-TF in the asymmetric unit. In both molecules only residues 4 to 208 of the crystallized fragment (residues 1 to 219) are visible in the electron density (Fig. 1). In addition, in molecule A (r-TF_A) residues 80, 81, 133, to 136 and 158 to 162 are missing, whereas in molecule B (r-TF_B) residues 79 to 81 and 158 to 162 were not modeled. The final model includes a total of 231 solvent molecules. Of these, 97 water molecules can be assigned to r-TF_A and 134 to r-TF_B on the basis of distances to the nearest protein atom.

Table 1. *Refinement statistics*

Model	
Total number of residues	391
Number of molecules in the crystallographic asymmetric unit	2
Number of solvent molecules	231
Total non-H atoms	3,407
Average *B*-factor molecule A and B (Å^2)	40.8, 28.5
Average *B*-factor of solvent molecules (Å^2)	38.8
Diffraction agreement	
Resolution (Å)	10.0–2.35
Completeness (%)	95.2
R-value (all data) (%)	19.1
R-value (2.46–2.35 Å) (%)	29.7
Number of reflections	18,203
Free *R*-value (10–2.35 Å) (%)	27.7
Free *R*-value (2.46–2.35 Å) (%)	34.6
Number of reflections	1,953
Anisotropic correction (Å^2)	
B11, B22, B33	2.6, 4.6, −7.2
B12, B13, B23	6.3, −8.5, 7.9
Stereochemistry	
RMSD in bonds (Å)	0.012
RMSD in angles (°)	1.61
RMSD in temperature factors of bonded atoms	
Overall (Å^2)	3.1
Main chain (Å^2)	1.8
Side chain (Å^2)	4.7

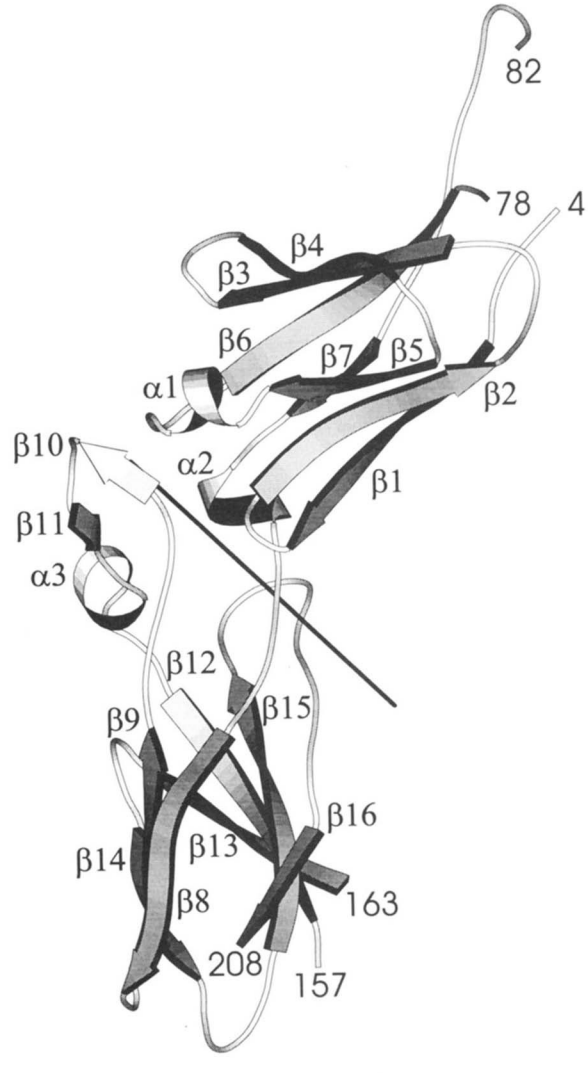

Fig. 1. Ribbon representation of the extracellular domain of r-TF generated with program Molscript (Kraulis, 1991). The hinge axis is indicated by a bold line. Secondary structure elements were assigned manually on the basis of dihedral angles and hydrogen bonding (distance cutoff; 3.5 Å), namely: $\beta 1$ = residues 8–15; $\beta 2$ = 18–24; $\beta 3$ = 31–38; $\beta 4$ = 44–50; $\beta 5$ = 53–57; $\alpha 1$ = 58–62; $\beta 6$ = 68–76; $\beta 7$ = 91–98; $\alpha 2$ = 100–104; $\beta 8$ = 110–117; $\beta 9$ = 120–126; $\beta 10$ = 132–134; $\beta 11$ = 137–139; $\alpha 3$ = 141–145; $\beta 12$ = 150–156; $\beta 13$ = 163–168; $\beta 14$ = 171–177; $\beta 15$ = 183–191; $\beta 16$ = 198–208. The "finger region" (segment $\beta 10$, $\beta 11$, $\alpha 3$) differs in both molecules in the asymmetric unit: In r-TF_B, in contrast to r-TF_A, residues 130–135 are not visible and hydrogen bonding between $\beta 10$ and $\beta 11$ shows that strand $\beta 10$ (residues 130–132 in r-TF_B) is shifted by two residues. With this single exception, secondary structure elements are identical in r-TF_A and r-TF_B and are identical to those observed in the crystal structure of h-TF (Muller et al., 1996).

The observed RMS deviations (RMSDs) from ideal stereochemistry (Engh & Huber, 1992) are 0.012 Å for bond lengths and 1.63° for bond angles, and are comparable to those observed for other crystal structures at medium resolution (Laskowski et al., 1993). Of all residues, 91.1% are located in the most favored region of the Ramachandran plot as deduced from a compilation of high resolution crystal structures (Laskowski et al., 1993). One residue is found in an unfavorable region (Fig. 2). Asn135 from r-TF_B, which is absent in the model of r-TF_A, is located at the tip of the finger region (see below) formed by strands β10 and β11 (Fig. 1). The equivalent residue in h-TF (Asn137) adopts similar unusual dihedral angles, both in the structure of the free protein (h-TF_{Free}) (Muller et al., 1996) and in the complex with FVIIa (h-TF_{FVIIa}) (Banner et al., 1996).

The average temperature factor (*B*-factor) is 34.9 $Å^2$. This is identical to the overall *B*-factor of 35.1 $Å^2$ as derived from a Wilson plot calculated between 4.3 and 2.35 Å resolution. The average *B*-factor of r-TF_A is higher than that of r-TF_B (40.8 $Å^2$ compared to 28.5 $Å^2$); this difference derives from differences in the mobility of the C-terminal domain (50.2 $Å^2$ compared to 29.4 $Å^2$). Although main-chain temperature factors within the C-terminal domain of r-TF_A reach values as high as 85 $Å^2$, the overall shape of the *B*-factor plot is very similar in both molecules, identifying identical loop regions as being highly mobile (data not shown).

Interestingly, the two molecules of r-TF pack in a pseudo-monoclinic arrangement in the crystal. They are related by an about 180° rotation around the *b*-axis, followed by a translation along this same axis of about 1/2 unit cell. The packing, however, rules out an alternative monoclinic space group assignment, as the *b* axis is not perpendicular to the *a*-*c* plane. As a consequence of the noncrystallographic screw axis along *b*, the observed crystal packing contacts along this direction are very similar for both molecules (see below).

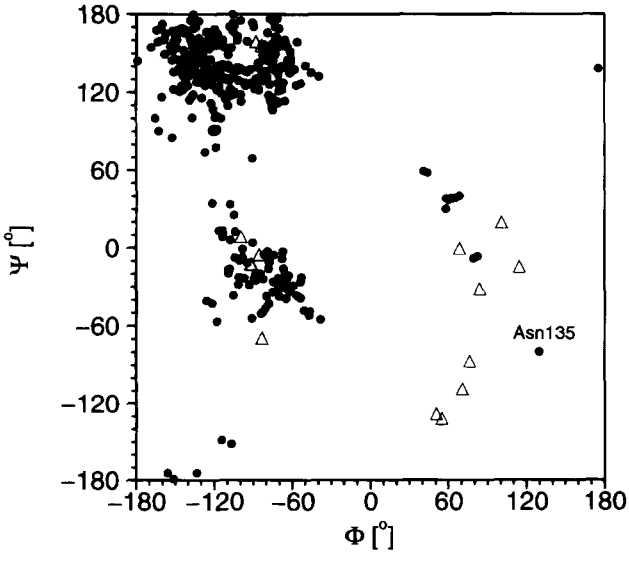

Fig. 2. Ramachandran representation of the dihedral angles ϕ ,ψ; nonglycine residues are indicated by dots, glycines by open triangles. Of all 391 residues, only Asn135 from molecule r-TF_B is located in a disallowed region of the Ramachandran plot as derived from a compilation of high resolution structures (Laskowski et al., 1993).

Overall structure

Like the human homologue, r-TF consists of two fibronectin type III (FNIII) modules that are linked by a short α-helix (Fig. 1). The FNIII fold consists of a four-stranded antiparallel β-sheet packed against a three-stranded β-sheet. The overall topology and strand connectivity are identical to those observed for the C2 subset of the Ig-Superfamily (Jones, 1993). However, sequence alignments and inspection of three-dimensional structures reveal that FNIII modules are characterized by a distinct packing of the hydrophobic core (Huber et al., 1994; Muller et al., 1996) and justify their classification as independent modules (Bork & Doolittle, 1992).

The FNIII domains in r-TF are very similar to each other. The N-terminal domain of r-TF can be superimposed on the C-terminal domain with an RMSD of 1.54 Å (57 C_α pairs) in r-TF_A and 1.65 Å (57 pairs) in r-TF_B. Features unique to the N-terminal domain are an additional short α-helix (α1) between strands β5 and β6 and a four residue long insertion between strands β6 and β7 (Fig. 1). Conversely, the C-terminal module contains a long insertion consisting of strands β10 and β11 and helix α3, which protrudes from the FNIII module, and has previously been named "finger region" (Harlos et al., 1994). This finger is observed only in molecule B, and is disordered in r-TF_A.

In both molecules, loop regions at the membrane side of the C-terminal FNIII module together with adjacent β-strand residues are associated with high temperature factors. Loop β12 to β13 is not visible in the electron density, and the loops connecting β8 to β9 and β14 to β15 constitute the regions with the highest temperature factors in r-TF_A and r-TF_B. Interestingly, an identical behavior is observed in the crystal structures of h-TF, both free (Muller et al., 1996) and in complex with FVIIa (Banner et al., 1996), showing that this reflects a general property of the molecule. It is known that the extracellular portion of TF by itself is less effective in activating FVIIa than membrane-bound, full-length TF, and that the activity depends on the phospholipid composition (Nemerson, 1995). We, therefore, speculate that this side of the molecule might gain structural stability from the direct interaction with the membrane. Alternatively, structural stability could arise from interaction with the substrate FX, as some residues nearby and within these loop regions have been proposed to interact with the latter (Kelley et al., 1995).

Domain–domain hinge bending

Like the interface in h-TF, the interface between the two FNIII modules of r-TF is predominantly composed of hydrophobic residues, and a continuous hydrophobic core extends from the N-terminal to the C-terminal domain. This observation, together with the absence of changes in domain–domain orientation upon binding of h-TF to FVIIa, suggests that the role of TF is to provide a rigid template for the binding of FVIIa (Banner et al., 1996). To our surprise, for r-TF there are clear differences in the domain–domain orientation between the two molecules in the asymmetric unit. When superimposing residues 6 to 210 of r-TF, the overall RMSD between r-TF_A and r-TF_B is 1.22 Å. Superposition of the N-terminal and C-terminal modules separately yields significantly lower RMSDs of 0.46 Å and 0.58 Å, respectively (Table 2).

The observed difference in the domain–domain orientation can be accurately described by a single hinge motion. Superposition of r-TF_B first onto the N-terminal domain of r-TF_A and subsequently onto the C-terminal domain of r-TF_A reveals a set of three atoms

Table 2. *Superposition of rabbit and human TF*[a]

	r-TF_A	r-TF_B	h-TF_{Free}	h-TF_{FVIIa}
r-TF_A		1.22/0.46/0.58	0.87/0.62/0.94	0.96/0.66/0.91
r-TF_B	186/99/92		1.32/0.56/1.07	1.02/0.69/0.98
h-TF_{Free}	177/90/88	178/88/88		0.86/0.63/0.91
h-TF_{FVIIa}	178/91/91	182/90/94	190/93/98	

[a]RMSDs (Å) obtained after superposition are listed above the diagonal. First number: RMSD after superposition of the entire extracellular domain; second and third numbers: RMSD after superposition of the N-terminal and C-terminal domain separately. Below the diagonal: number of C_α atoms used in the superposition after applying a distance cutoff of 3.0 Å in program O (Jones et al., 1991).

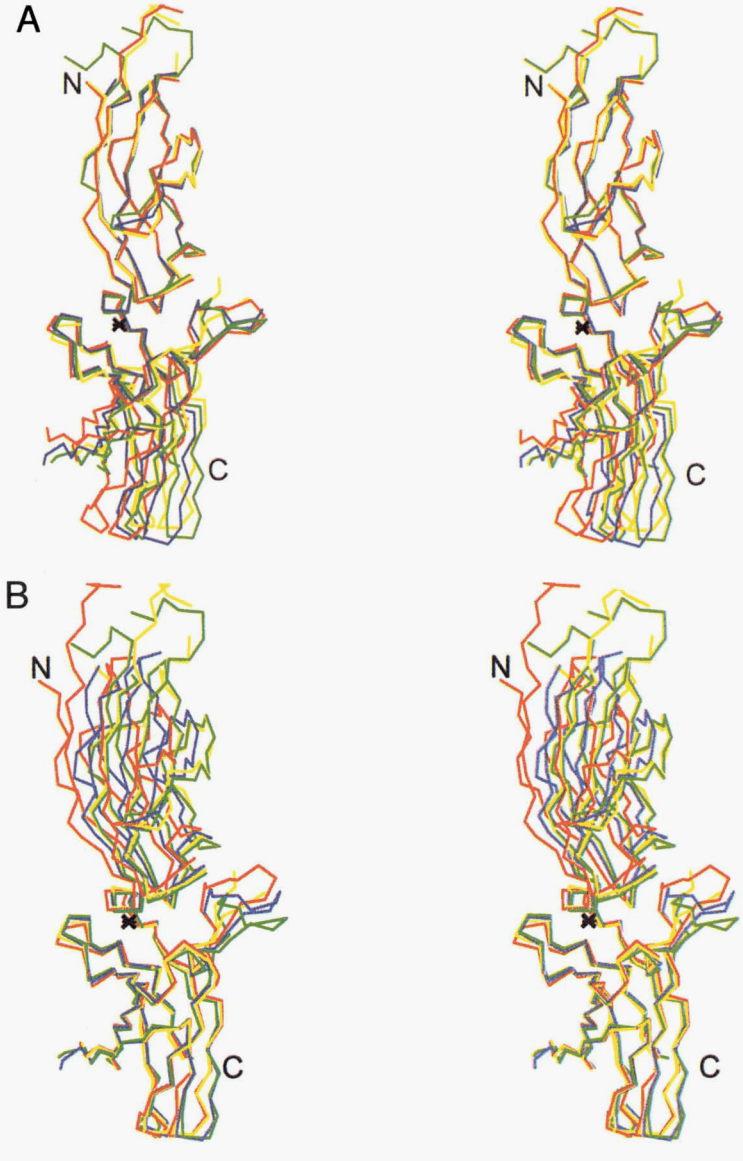

Fig. 3. Stereo C_α representation of r-TF_B (red), h-TF_{Free} (green), and h-TF_{FVIIa} (blue) superimposed on (**A**) the N-terminal domain of r-TF_A (yellow) and (**B**) the C-terminal domain of r-TF_A. The orientation of the molecule is identical to the orientation shown in Figure 1 following a 90° rotation along a vertical axis and viewing down the hinge axis (black cross).

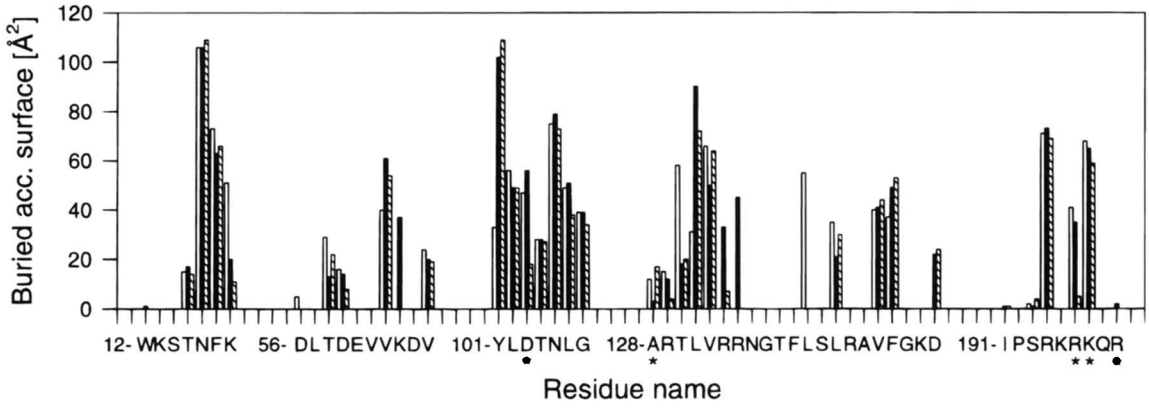

Fig. 4. Surface area buried within the domain–domain interface per residue (r-TF_A, white bars; r-TF_B, black bars; and r-TF_{Free}, hashed bars). Residues that differ in sequence between rabbit and human are marked with asterisks (see Fig. 6). The surface area is overemphasized for residues 105 and 106; to delimit the N- and C-terminal domain the peptide bond in between has been artificially broken.

in r-TF_B whose coordinates move by a mere 0.17 Å (less than the estimated average coordinate error) upon application of the second transformation. These atoms are Tyr101-CG, Leu106-N, and Pro201-CG. They define the direction of a hinge-axis, and a rotation of 12.7° around this axis relates the domain–domain orientation observed in r-TF_A to the orientation in r-TF_B (Fig. 3). The hinge axis passes through Leu106-N, which is part of the main chain of the linker segment. However, it is not possible to relate both orientations by a single rotation around the ϕ angle of Leu106; slight adjustments have to occur in the dihedral angles of the entire linker segment. It is noteworthy that in r-TF the differences can be explained by a single hinge motion rather than a combination of shear and hinge motion (Gerstein et al., 1994).

To accommodate the hinge motion only minor rearrangements within the interface are necessary. The total surface area buried in the interface is very similar between r-TF_A and r-TF_B, namely 660 and 610 $Å^2$, respectively (Fig. 4). With the exception of segment β10 to β11, only small differences in buried surface area are observed for individual residues. As shown in Figure 5, the reorientation of the N-terminal domain is accompanied by a slight displacement of loops β10 to β11 and β15 to β16 of the C-terminal domain. The only significant difference in side-chain conformations is observed for Tyr101. In r-TF_B the side chain of Tyr101 is hydrogen bonded to Asp148, while in r-TF_A, χ1 is rotated by about 120°, and the side chain is pointing towards the solvent (Fig. 5).

It could be argued that the observed hinge motion is induced by crystal packing forces. However, we rather believe that crystal packing constraints help to stabilize the conformational diversity. A major contact of about 370 $Å^2$ is formed between residues in the interface region of r-TF_A and residues 48 and 49 of a neighboring r-TF_B molecule. As a consequence of the pseudo-2_1-screw axis along the crystallographic *b* axis, a very similar but even larger contact (540 $Å^2$) is observed for residues involving the interface region of r-TF_B.

Comparison between rabbit TF and human TF

Of the 217 common residues in the extracellular portion of TF, 75% are identical between the rabbit and human proteins. Of the58 substitutions, most are conservative and the majority are found on

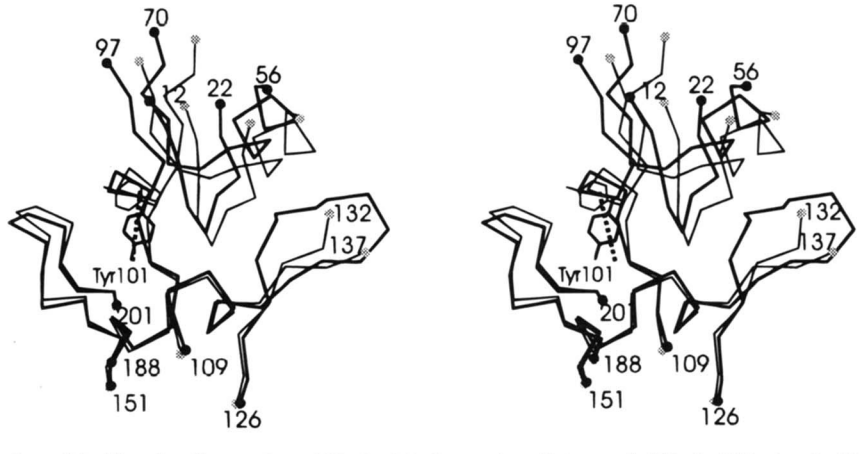

Fig. 5. Detailed view of the hinge bending motion within the interface region. C_α trace of r-TF_B (bold line) and r-TF_A (thin line) after superposition of the C-terminal domains and in an orientation similar to Figure 4B. The only major difference between r-TF_A and r-TF_B in the interface region is the orientation of the side chain of Tyr101. In r-TF_B, Tyr101-Oη is hydrogen bonded to Asp148-Oδ1 of the C-terminal domain. This interaction is absent in r-TF_A. The hinge axis is shown as a bold dashed line.

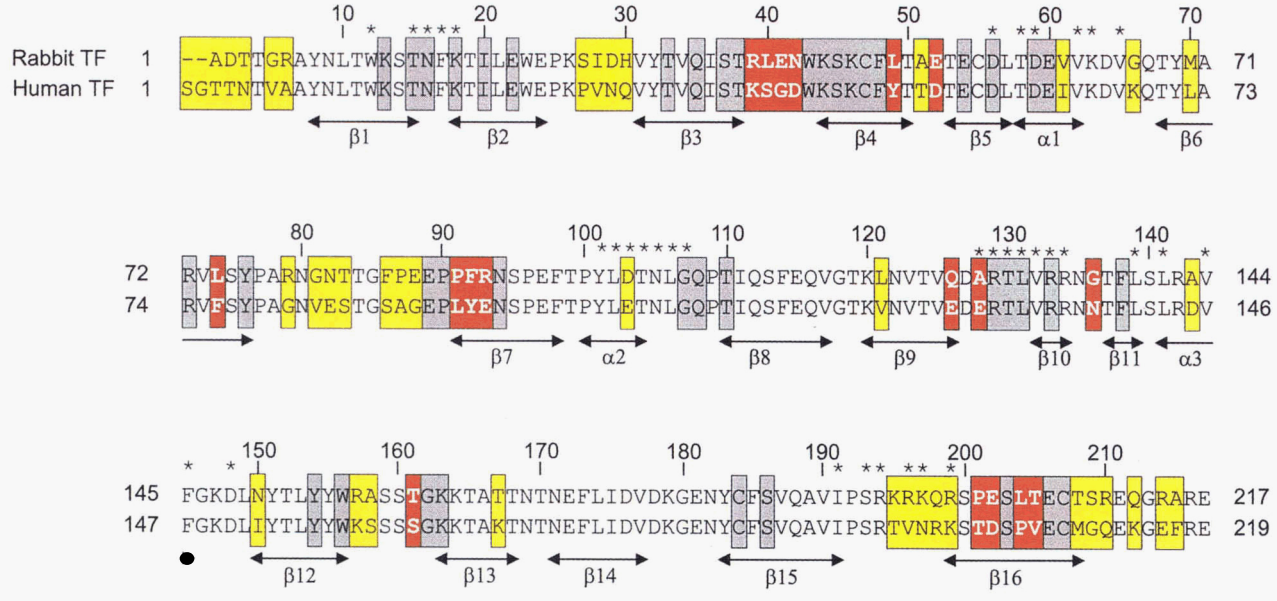

Fig. 6. Sequence alignment of r-TF and h-TF. Yellow boxes: residues that differ in sequence between r-TF and h-TF; gray boxes: residues of h-TF buried in the interface between TF and FVIIa as observed in the crystal structure of the complex TF·FVIIa (Banner et al., 1996). In red: residues that are both buried in the interface and differ in sequence. Secondary structure elements are shown as two-headed arrows. Asterisks denote residues contributing to the intramolecular interface between the N- and C-terminal FNIII domain of TF.

the surface and in exposed loop regions (Fig. 6). One substitution (Leu121 to valine in h-TF) is observed at the boundary between surface and hydrophobic core and five substitutions are observed at the periphery of the interface between the N- and C-terminal domain. For the individual FNIII modules, only a small number of differences in the main-chain conformation between r-TF and h-TF are observed. The large deviations in segment 82 to 90 of the N-terminal domain result from crystal packing artifacts, and in all crystal structures of TF this segment lacks secondary structure elements and is only observable if the segment interacts with neighboring molecules in the crystal. Deviations as large as 6.3 Å between equivalent C_α positions are observed for loop β3 to β4 in the N-terminal domain and as large as 3.1 Å for loop β10 to β11 in the C-terminal domain (Fig. 3). Five residues in loop β3 to β4 differ in sequence between r-TF and h-TF, and the observed difference in main-chain conformation results from the substitution of Glu41 to glycine in the human sequence, conferring greater local flexibility to the main chain. Loop β10 to β11 deviates quite significantly between the two r-TF as well as the two h-TF structures, making a direct comparison between the rabbit and human proteins impossible. In general, the RMSDs observed for the superposition of the N-terminal domains are lower than those observed for the C-terminal domains (Table 2), consistent with the lower average temperature factors of the N-terminal domains. The deviations observed between r-TF and h-TF for the single domains are similar to those between h-TF_{Free} and h-TF_{FVIIa}.

The observation that r-TF_A and r-TF_B differ in their domain–domain orientation prompted us to compare the orientations in all four structures of TF reported to date, that is, r-TF_A, r-TF_B, h-TF_{Free} and h-TF_{FVIIa}. Comparing the RMSDs for the entire extracellular portion shows that h-TF_{Free} is closely similar to r-TF_A, with an RMSD of 0.87 Å (Table 2), but differs significantly from r-TF_B (RMSD 1.32 Å). h-TF_{FVIIa} differs equally from r-TF_A and r-TF_B (RMSD 0.96 Å and 1.02 Å, respectively), however, it superimposes well with h-TF_{Free} (RMSD 0.86 Å). In most cases, the RMSDs observed for the C-terminal domain alone are as high as the deviations observed when superimposing the entire extracellular portion (Table 2).

A clear picture emerges when comparing the relative hinge angles among the different structures (Table 3). The hinge angles show that r-TF_A and r-TF_B represent two border structures, and while the hinge angle of h-TF_{Free} resembles the domain orientation in r-TF_A, the hinge angle of h-TF_{FVIIa} represents an intermediate between the two border structures. These effects are very nearly additive, the hinge angle difference between r-TF_A and r-TF_B (12.7°) closely approximating the sum (13.7°) of the hinge angle differences between r-TF_A and h-TF_{Free} (3.7°), h-TF_{Free} and h-TF_{FVIIa} (3.5°), and h-TF_{FVIIa} and r-TF_B (6.5°). This additivity of the observed effects supports the postulation of a unique hinge motion in all TF structures. Furthermore, our analysis detects a heretofore unnoticed difference between free and bound h-TF. Thus, in contrast to the previous concept of TF being a rigid template for binding FVIIa, it is likely that a range of possible conformations about the hinge axis exists for free TF in solution, and that the conformation observed in the h-TF·FVIIa complex is selected by FVIIa binding.

Table 3. *Relative hinge angles observed in tissue factor*[a]

	r-TF_B	h-TF_{Free}	h-TF_{FVIIa}
r-TF_A	12.7	3.7	7.3
r-TF_B		11.8	6.5
h-TF_{Free}			3.5

[a]The relative hinge angle (°) is defined as the rotation required to superimpose the second domain following superposition of the first domain.

FVIIa activation

rTFAA binds to human FVIIa (h-FVIIa) with a threefold decrease in affinity when compared to hTFAA (Kelley et al., 1997). Relating the sequence differences observed between r-TF and h-TF to the amino acids participating in the interface between h-TF and h-FVIIa identifies four regions of interest (Figs. 6, 7). These regions are Arg39 to Asn42, Leu74, Pro91 to Arg93, and Pro201 to Thr205 (r-TF numbering). In the structure of h-TF_{FVIIa} (Banner et al., 1996), segment Arg39 to Asn42 is mainly involved in main-chain contacts to h-FVIIa; therefore, substitutions within this segment should not affect binding. However, because Gly41 of h-TF is substituted by glutamine in the rabbit sequence, the overall flexibility of this loop might be altered; moreover, substitution of nearby residue Asp44 of h-TF to alanine results in a modest decrease in affinity (Kelley et al., 1995). The segment centered on Leu74 appears to be important for specificity. In the structure of the h-TF·h-FVIIa complex, Phe76 of h-TF is in contact with Phe129f and Met164 of the proteolytic domain of FVIIa (see Bode et al., 1989 for standard serine protease numbering convention). Alanine substitution of Phe76 results in a 20-fold decrease in binding affinity (R. Kelley, unpubl. obs.); furthermore, Phe129f is replaced by threonine in rabbit FVIIa (r-FVIIa). Within the segment Pro91 to Arg93, Tyr92 (which is substituted to phenylalanine in r-TF) is buried in a hydrophobic pocket in the h-TF·h-FVIIa complex, and the hydroxyl group of the tyrosine side chain makes a hydrogen bond to the main chain of FVIIa. In h-TF, the Y92A mutation results in a large decrease in binding (Kelley et al., 1995), showing that the side chain at this position is important. Although the difference between tyrosine and phenylalanine is subtle, the absence of the hydroxyl group in r-TF would result in a loss of this hydrogen bond and could therefore decrease the binding affinity of r-TF toward h-FVIIa. Interestingly, the loop segment that forms the hydrophobic pocket in FVIIa is close to its active site, and it has been suggested that conformational changes induced by TF in this segment play an essential role in the activation of FVIIa (Banner et al., 1996). Finally, in the segment Pro201 to Thr205 most side chains are involved in hydrophobic contacts with h-FVIIa, and the structure of the complex suggests that the substitutions could be easily accommodated. Indeed, alanine substitutions within this region in h-TF have little effect on binding to h-FVIIa (Kelley et al., 1995). However, Val205, which is threonine in the rabbit sequence, is completely buried in a hydrophobic pocket in the h-TF·h-FVIIa interface. The substitution of a methyl group by a hydroxyl group in case of r-TF generates an unbalanced hydrogen bond and thus might decrease the binding affinity. In this context, it is noteworthy that the hydrophobic pocket that surrounds Thr205 of r-TF in the complex with h-FVIIa is modified in the rabbit protease to provide a hydrogen bonding acceptor, as Leu39 is substituted with glutamine in r-FVIIa.

No direct affinity measurements are available for binding of h-TF to r-FVIIa, because purified r-FVIIa is not available. However, a 70-fold decrease in the anticoagulant activity of the double mutant hTFAA has been observed in rabbit plasma when compared to human plasma (Kelley et al., 1997). As the anticoagulant effect is shown to result from the formation of inactive TFAA·FVIIa complexes, it can be anticipated that the binding affinity of hTFAA to r-FVIIa is considerably reduced. Based on the analysis presented above, the residues of h-TF most likely to be responsible for the decreased affinity for r-FVIIa are the 41 to 44 loop and Phe76. We have tested this hypothesis by replacing these residues in hTFAA with the corresponding rabbit sequence. Substitution of the loop resulted in a variant that expressed poorly and could not be further characterized. As for Phe76, the F76L mutant of hTFAA retained good anticoagulant properties in human plasma, while having greater potency in rabbit plasma relative to hTFAA (Fig. 8). Although this mutant is still a less potent anticoagulant in rabbit plasma than rTFAA, it is clear that changes at the key contacts described above can be used to increase binding to r-FVIIa, and that important specificity determinants reside among these residues.

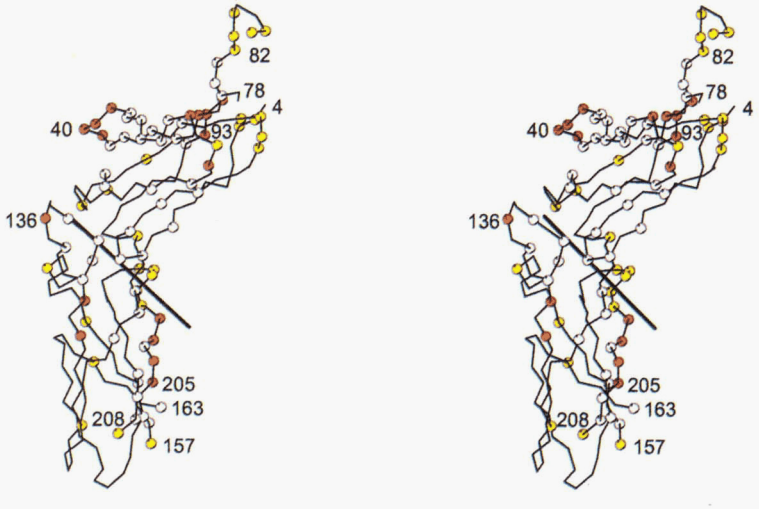

Fig. 7. Stereo C_α representation of the extracellular domain of r-TF emphasizing residues that differ in sequence between rabbit and human TF (yellow spheres). Residues of h-TF buried in the complex with TF·FVIIa (Banner et al., 1996) are shown as white spheres. Residues that are both buried in the complex and differ in sequence between r-TF and h-TF and which, therefore, could explain differences observed in the cofactor activity are shown in red. The hinge axis is indicated as a bold line. In addition to the termini, several residues are labeled for convenience.

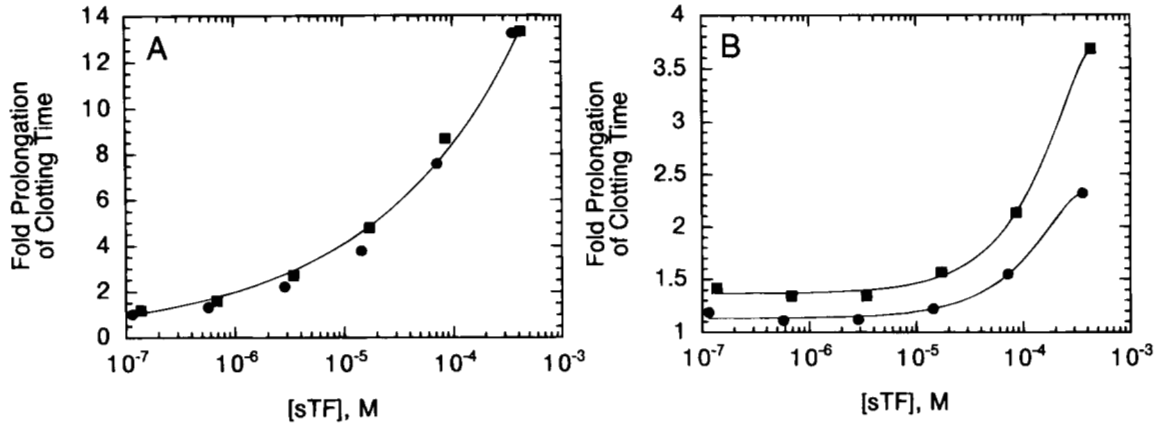

Fig. 8. Comparison of the anticoagulant properties of hTFAA (circles) and F76L-hTFAA (squares) in human (**A**) and rabbit (**B**) plasma. TFAA variants were expressed by secretion from *E. coli*, purified, and tested for inhibition of TF-dependent clotting (prothrombin time assay) as previously described (Kelley et al., 1997).

Implications for other cytokine receptors

Tissue factor is a member of Class II of the cytokine receptor super-family, to which also belong the α-, β-, and γ-interferon and interleukin-10 receptors. A comparison between crystal structures of members of Class II and those of Class I, which includes the growth hormone, prolactin, and erythropoietin receptors, has revealed that a distinguishing structural difference between the two classes appears to be the relative orientation between the N- and C-terminal domains (Kossiakoff et al., 1994; Muller et al., 1994; Walter et al., 1995). However, with the exception of h-TF, all presently known structures were determined for ligand-bound receptors, and no free receptor structures have thus far been published. Thus, it is unknown whether ligand binding is accompanied by changes in the relative orientation between the two domains, or whether the receptors represent rigid templates for ligand binding. It is noteworthy that in contrast to the interface in tissue factor, the domain–domain interface in members of Class I is not hydrophobic in nature, and therefore, not a continuation of the hydrophobic cores of the individual domains. In light of this, our finding of unexpected and relatively large hinge bending movement around a well-defined axis in TF makes it tempting to suggest that similar flexibility is likely to exist for other receptors within the superfamily, and that the orientation observed in the complexes is induced and/or stabilized by ligand binding. In the absence of additional experimental data it is impossible to decide on the magnitude of these changes or the position of the putative hinge axis; more precise answers will have to await determination of the structure of a free receptor.

Materials and methods

Protein expression and purification

Wild-type, soluble rabbit tissue factor (residues 1–219) was expressed and purified by using a protocol previously described for rTFAA (Kelley et al., 1997). Purified r-TF appeared homogeneous by SDS-PAGE (>90% purity), and gave a molecular weight of 24,881 ± 2.2 Da upon electrospray-ionization mass spectrometry (Bourrell et al., 1994), consistent with the molecular weight calculated from the amino acid sequence (24,880.79 Da; data not shown).

Crystallization and data collection

Initial microcrystals were obtained using the hanging drop method and a commercial crystallization screen (Hampton Research, USA) (Jancarik & Kim, 1991). These crystals consisted of bushes of thin, two-dimensional plates, and grew from 30% PEG 4000, 0.1 M TRIS·HCl, 0.2 M Li_2SO_4, pH 8.5 as a precipitation solution. Single crystals were obtained using the sitting drop method and after macroseeding into a droplet of 80 μL of protein solution (10 mg/mL protein in 50 mM TRIS·HCl, pH 8.0, 50 mM NaCl, 75 mM Li_2SO_4, 12.5% PEG 3350) and equilibrating against 30 mL of reservoir solution (50 mM TRIS·HCl, pH 8.0, 50 mM NaCl, 150 mM Li_2SO_4, 25% PEG 3350) with fragments of the initial microcrystals. The resulting crystals were still rather thin and reached a typical size of $600 \times 600 \times 50$ μm^3. The crystals could be flash cooled at 100 K after being transferred into 100 μL of reservoir solution that had been brought to 6% of 2-methyl 2,4-pentanediol.

An initial data set to 2.6 Å resolution was collected from a single crystal on a MAR image plate mounted on a Rigaku RU200 rotating anode with CuKα radiation (Table 4). The crystal belonged to space group $P1$ with cell parameters $a = 42.54$ Å, $b = 49.01$ Å, $c = 65.01$ Å, $\alpha = 96.06°$, $\beta = 99.11°$, $\gamma = 91.14°$, and contained two molecules in the unit cell (corresponding to a V_M of 2.7 $Å^3$ Da^{-1} (Matthews, 1968) and a solvent content of 54%). Following data collection, the crystal was stored in liquid nitrogen, and later used to collect the final data set to 2.35 Å at the Cornell High Energy Synchrotron Source, beam line F1. A total of 200 images with a 1° rotation step each were collected with the Princeton CCD detector at a crystal to detector distance of 70 mm using a wavelength of 0.909 Å. Low-resolution data were obtained from an additional set of 100 images with shorter exposure times and 2° rotation steps at a crystal detector distance of 120 mm. Both series of images were processed independently with programs DENZO and SCALEPACK (Otwinowski, 1993), and the unique reflection files were scaled together with program SCALEPACK. A total of 62,914 reflections were reduced to 20,678 unique reflections; the

Table 4. *Data statistics*

Data set 1							
Resolution shell (Å)	60–4.5	4.5–3.6	3.6–3.2	3.2–2.9	2.9–2.7	2.7–2.55	Overall
R_{sym}[a] (%)	2.5	3.5	4.7	7.0	9.3	13.3	4.4
Completeness (%)	93.3	92.3	91.4	92.1	91.9	90.6	92.0
Completeness $I > 3\sigma$	92.5	89.3	86.7	82.4	80.1	75.9	84.7
Redundancy	1.9	1.9	1.9	1.9	1.9	1.9	1.9
Data set 2							
Low-resolution data collection							
Resolution shell (Å)	60–3.7	3.7–3.1	3.1–2.8	2.8–2.7	2.7–2.6	2.6–2.5	Overall
R_{sym} (%)	3.2	3.9	5.2	6.4	8.4	9.4	3.6
Completeness (%)	95.9	96.7	94.9	79.1	56.1	31.2	83.8
Completeness $I > 3\sigma$	94.0	93.2	85.0	64.8	42.9	23.6	77.0
Redundancy	2.0	2.0	1.8	1.6	1.6	1.6	1.9
High-resolution data collection							
Resolution shell (Å)	60–4.0	4.0–3.2	3.2–2.8	2.8–2.5	2.5–2.4	2.4–2.35	Overall
R_{sym} (%)	4.4	4.8	4.8	5.4	5.7	6.9	5.0
Completeness (%)	58.7	62.3	97.4	97.6	97.4	90.6	82.0
Completeness $I > 3\sigma$ (%)	58.1	61.3	94.9	91.9	87.8	86.7	77.7
Redundancy	1.8	2.1	2.1	2.1	2.1	2.0	2.0
Combined data							
Resolution shell (Å)	60–4.0	4.0–3.2	3.2–2.8	2.8–2.6	2.6–2.5	2.5–2.35	Overall
R_{merge}[a] (%)	9.0	6.8	6.8	7.7	9.1	—	7.5
Completeness (%)	97.2	96.3	98.5	98.0	97.4	89.5	96.4
Number of unique reflections	4,184	4,129	4,233	2,788	2,790	2,554	20,678

[a] R_{sym} and R_{merge} are defined as follows: $R_{sym} = 100 \cdot \Sigma|I_i - \langle I \rangle| / \Sigma I_i$, $R_{merge} = 100 \cdot \Sigma|I_1 - I_2| / \Sigma(I_1 + I_2)$.

final data set was 96.4% complete in the resolution range between 60 and 2.35 Å.

Structure determination and refinement

The structure of r-TF was solved by molecular replacement using the structure of the extracellular portion of h-TF as a search model (protein databank entry code 2hft, Muller et al., 1996). A conventional rotation search with program AMORE (CCP4, 1994) failed to identify a rotation solution for the second molecule in the asymmetric unit. The rotation solutions for both molecules stood out clearly after Patterson correlation refinement with program XPLOR (Brünger et al., 1987; Brünger, 1990) and after allowing the N- and C-terminal domains to adjust independently. The rotation search was calculated in the resolution range 10 to 4 Å and using an integration sphere of 12 Å radius, giving solutions with correlation coefficients of 0.27 and 0.22 compared to the highest noise peak at 0.12.

The translation search was calculated with program AMORE using the same resolution range as for the rotation search. The correct translation of the second molecule, fixing the first molecule arbitrarily at the origin, resulted in an R-value of 45.4% and a correlation coefficient of 0.465, with the highest noise peak having an R-value and correlation coefficient of 51.4% and 0.30, respectively. Inspection of the resulting solution with program O (Jones et al., 1991) revealed a convincing packing scheme and the absence of stereochemical clashes.

The model was initially refined against the 2.6 Å resolution data set. After rigid body and positional refinement, the R-value dropped to 36.3% (with a free R of 42.2%) in the resolution range 10 to 3.0 Å, and clear difference density was visible at positions where the sequence of r-TF differs from the sequence of the human homologue. The changes were incorporated into the model and refinement continued by alternating steps of model rebuilding using program O (Jones et al., 1991) with conventional refinement using program XPLOR (Brünger et al., 1987). Noncrystallographic symmetry restraints were introduced between the two molecules in the asymmetric unit, restraining the N-terminal domains separately from the C-terminal domains and omitting loop regions, which clearly differed in their conformations. In the final refinement rounds, using the high-resolution data set and after extending the resolution to 2.35 Å, program REFMAC (CCP4, 1994) was used for several cycles. Toward the end of refinement, an explicit bulk solvent correction calculated with XPLOR was introduced into REFMAC using partial structure factors. In addition, the dataset was corrected for observed anisotropy using program XPLOR (Table 1). At the end of the refinement noncrystallographic symmetry restraints were removed.

Solvent molecules were incorporated into the model after the R-value dropped to 27.4% (free R-value 33.7%). Only peak positions higher than 3.5σ in the Sigmaa-weighted difference density map (Read, 1986) and with reasonable geometry were considered. Solvent molecules were removed if their temperature factors exceeded 80 Å^2 or displayed less than 1σ density in the resulting $2F_o - F_c$ electron density map. Refinement converged at an R-value of 19.6% (free R-value 27.7%), and no interpretable difference density remained in the final $(F_o - F_c) \cdot \exp(i\alpha_c)$ electron density map.

Structure superpositions, determination of hinge angles, and location of the hinge axis

All superpositions were optimized using program O (Jones et al., 1991) by first explicitly stating the C_α positions used for superposition (option LSQ_EXPLICIT) and subsequent iterative determination of the best subset of atoms within a distance cutoff of 3.0 Å (option LSQ_IMPROVE). The relative hinge angles between two molecules were calculated by first superimposing a

single domain, followed by calculation of the rotation angle required to achieve optimal superposition of the second domain (program LSQMAN; CCP4, 1994). The location of the hinge axis within r-TF was calculated as follows: first r-TF_B was superimposed onto the C-terminal domain of r-TF_A, then the transformation was calculated to achieve superposition of the N-terminal domain, and a set of three atoms identified whose coordinates were almost invariant to this transformation. These coordinates were used as starting points for an iterative search for positions for which the difference between the transformed and starting coordinates was minimized and thus by definition are located on the rotation axis. The coordinates of h-TF_{FVIIa} (Banner et al., 1996) were obtained from the protein data bank (accession code 1dan).

Coordinates and structure factor amplitudes of r-TF have been deposited with the protein data bank (accession code 1a21).

Note added in proof

After submission of this paper, Huang et al. published a crystallographic investigation on the crystal structures of h-TF alone and in complex with a FAB fragment. They observe a similar albeit smaller (7°) variation in the hinge angle of h-TF when comparing their model to previously published h-TF structures. (Huang M, Syed R, Stura EA, Stone MJ, Stefanko RS, Ruf W, Edgington TS, Wilson IA. 1998. The mechanism of an inhibitory antibody on TF initiated blood coagulation revealed by the crystal structures of human tissue factor, FAB 5G9 and TF·FAB 5G9 complex. *J Mol Biol 275*:873–894.)

Acknowledgments

We thank the staff at CHESS for help with beam line F1, Michael Randal, Charles Eigenbrot, and Patricia Elkins at Genentech, Inc., for help with data collection, and Udo Heinemann from the Forschungsgruppe Kristallographie for generous support and critical reading of the manuscript. Y.A.M. was supported by a grant from the European Community (BIO4CT965090).

References

Banner DW, D'Arcy A, Chene C, Winkler FK, Guha A, Konigsberg WH, Nemerson Y, Kirchhofer D. 1996. The crystal structure of the complex of blood coagulation factor VIIa with soluble tissue factor. *Nature 380*:41–46.

Bazan JF. 1990. Structural design and molecular evolution of a cytokine receptor superfamily. *Proc Natl Acad Sci USA 87*:6934–6938.

Bode W, Mayr I, Baumann U, Huber R, Stone SR, Hofsteenge J. 1989. The refined 1.9 Å crystal structure of human alpha-thrombin: Interaction with D-Phe-Pro-Arg chloromethylketone and significance of the Tyr-Pro-Pro-Trp insertion segment. *EMBO J 8*:3467–3475.

Bom VJ, Bertina RM. 1990. The contribution of Ca^{2+}, phospholipids and tissue-factor apoprotein to the activation of human blood-coagulation factor X by activated factor VII. *Biochem J 265*:327–336.

Bork P, Doolittle RF. 1992. Proposed acquisition of an animal protein domain by bacteria. *Proc Natl Acad Sci USA 89*:8990–8994.

Bourrell JH, Clauser KP, Kelley R, Carter P, Stults JT. 1994. Electrospray ionization mass spectrometry of recombinantly engineered antibody fragments. *Anal Chem 66*:2088–2095.

Brünger AT. 1990. Extension of molecular replacement: A new search strategy based on the Patterson correlation refinement. *Acta Crystallogr A46*:46–57.

Brünger AT, Kuriyan J, Karplus M. 1987. Crystallographic R factor refinement by molecular dynamics. *Science 235*:458–460.

CCP4. 1994. The CCP4 suite: Programs for protein crystallography. *Acta Crystallogr D50*:760–763.

Davie EW, Fujikawa K, Kisiel W. 1991. The coagulation cascade: Initiation, maintenance, and regulation. *Biochemistry 30*:10363–10370.

Dickinson CD, Kelly CR, Ruf W. 1996. Identification of surface residues mediating tissue factor binding and catalytic function of the serine protease factor VIIa. *Proc Natl Acad Sci USA 93*:14379–14384.

Engh RA, Huber R. 1992. Accurate bond and angle parameters for X-ray protein-structure refinement. *Acta Crystallogr A47*:392–400.

Gerstein M, Lesk AM, Chothia C. 1994. Structural mechanisms for domain movements in proteins. *Biochemistry 33*:6739–6749.

Harlos K, Martin DMA, O'Brien DP, Jones EY, Stuart DI, Polikarpov I, Miller A, Tuddenham, EGD, Boys CWG. 1994. Crystal structure of the extracellular region of human tissue factor. *Nature 370*:662–666.

Higashi S, Matsumoto N, Iwanaga S. 1996. Molecular mechanism of tissue factor-mediated acceleration of factor VIIa activity. *J Biol Chem 271*:26569–26574.

Huber AH, Wang Y-ME, Bieber AJ, Bjorkman PJ. 1994. Crystal structure of tandem type III fibronectin domains from *Drosophila* neuroglian at 2.0 A. *Neuron 12*:717–731.

Jancarik J, Kim SH. 1991. Sparse matrix sampling: A screening method for crystallization of proteins. *J Appl Crystallogr 24*:409–411.

Jones EY. 1993. The immunoglobulin superfamily. *Curr Opin Struct Biol 3*:846–852.

Jones TA, Zou J-Y, Cowan SW, Kjeldgaard M. 1991. Improved methods for building protein models in electron density maps and the location of errors in these models. *Acta Crystallogr A47*:110–119.

Kelley RF, Costas KE, O'Connell MP, Lazarus RA. 1995. Analysis of the factor VIIa binding site on human tissue factor: Effects of tissue factor mutations on the kinetics and thermodynamics of binding. *Biochemistry 34*:10383–10392.

Kelley RF, Refino CJ, O'Connell MP, Modi N, Sehl P, Lowe D, Pater C, Bunting S. 1997. A soluble tissue factor mutant is a selective anticoagulant and antithrombotic agent. *Blood 89*:3219–3227.

Kossiakoff AA, Somers W, Ultsch M, Andow K, Muller YA, de Vos AM. 1994. Comparison of the intermediate complex of human growth hormone bound to the human growth hormone and prolactin receptors. *Protein Sci 3*:1697–1705.

Kraulis PJ. 1991. MOLSCRIPT: A program to produce both detailed and schematic plots of protein structures. *J Appl Crystallogr 24*:946–950.

Laskowski RA, MacArthur MW, Moss DS, Thornton JM. 1993. Procheck: A program to check the stereochemical quality of protein structures. *J Appl Crystallogr 26*:283–291.

Luzzati PV. 1952. Traitement statistique des erreurs dans la determination des structures cristallines. *Acta Crystallogr 5*:802–810.

Matthews BW. 1968. Solvent content of protein crystals. *J Mol Biol 33*:491–497.

Morrissey JH, Fakhrai H, Edgington TS. 1987. Molecular cloning of the cDNA for tissue factor, the cellular receptor for the initiation of the coagulation protease cascade. *Cell 50*:129–135.

Muller YA, Ultsch MH, de Vos AM. 1996. The crystal structure of the extracellular domain of human tissue factor refined to 1.7 Å resolution. *J Mol Biol 256*:144–159.

Muller YA, Ultsch MH, Kelly RF, de Vos AM. 1994. Structure of the extracellular domain of human tissue factor: Location of the factor VIIa binding site. *Biochemistry 33*:10864–10870.

Nemerson Y. 1995. Tissue factor: Then and now. *Thromb Haemost 74*:180–184.

Otwinowski Z. 1993. Oscillation data reduction program. In: Sawyer L, Isaacs N, Bailey S, eds. *Proceedings of the CCP4 study weekend: Data collection and processing*. UK: SERC Daresbury Laboratory. pp 56–62.

Pawashe AB, Golino P, Ambrosio G, Miglliaccio F, Ragni M, Pascucci I, Chiariello M, Bach R, Garen A, Konigsberg WH, Ezekowitz MD. 1994. A monoclonal antibody against rabbit tissue factor inhibits thrombus formation in stenotic injured rabbit carotid arteries. *Circ Res 74*:56.

Read RJ. 1986. Improved Fourier coefficients for maps using partial structures with errors. *Acta Crystallogr A42*:140–149.

Rottingen JA, Enden T, Camerer E, Iversen J, Prydz H. 1995. Binding of human factor VIIa to tissue factor induces cytosolic Ca^{2+} signals in J82 cells, transfected COS-1 cells, MDCK cells and in human endothelial cells induced to synthesize tissue factor. *J Biol Chem 270*:4650–4660.

Scarpati EM, Wen D, Broze GJ Jr, Miletich JP, Flandermeyer RR, Siegel NR, Sadler JE. 1987. Human tissue factor: cDNA sequence and chromosome localization of the gene. *Biochemistry 26*:5234–5238.

Taylor FB, Chang A, Ruf W, Morrissey JH, Hinshaw L, Catlett R, Blick K, Edgington TS. 1991. Lethal *E. coli* septic shock is prevented by blocking tissue factor with monoclonal antibody. *Circ Shock 33*:127.

Walter MR, Windsor WT, Nagabhushan TL, Lundell DJ, Lunn CA, Zauodny PJ, Narula SK. 1995. Crystal structure of a complex between interferon-γ and its soluble high-affinity receptor. *Nature 376*:230–235.

Wells JA, de Vos AM. 1996. Hematopoietic receptor complexes. *Annu Rev Biochem 65*:609–634.

Zioncheck TF, Roy S, Vehar GA. 1992. The cytoplasmic domain of tissue factor is phosphorylated by a protein kinase C-dependent mechanism. *J Biol Chem 267*:3561–3564.